

Exact spectral properties of Fermi polarons in one-dimensional lattices: Anomalous Fermi singularities and polaron quasiparticles

Hui Hu,¹ Jia Wang,¹ and Xia-Ji Liu¹

¹*Centre for Quantum Technology Theory, Swinburne University of Technology, Melbourne 3122, Australia*
(Dated: April 8, 2025)

We calculate the exact spectral function of a single impurity repulsively interacting with a bath of fermions in one-dimensional lattices, by deriving the explicit expression of the form factor for both regular Bethe states and the irregular spin-flip state and η -pairing state, based on the exactly solvable one-dimensional Hubbard model. While at low impurity momentum $Q \sim 0$ the spectral function is dominated by two power-law Fermi singularities, at large momentum we observe that the two singularities develop into two-sided distributions and eventually become anomalous Fermi singularities at the boundary of the Brillouin zone (i.e., $Q = \pm\pi$), with the power-law tails extending towards low energy. Near the quarter filling of the Fermi bath, we also find two broad polaron peaks at large impurity momentum, collectively contributed by many excited many-body states with non-negligible form factors. Our exact results of those distinct features in one-dimensional Fermi polarons, which have no correspondences in two and three dimensions, could be readily probed in cold-atom laboratories by trapping highly imbalanced two-component fermionic atoms into one-dimensional optical lattices.

The motion of an impurity interacting with a Fermi bath is a paradigm in many-body physics and condensed matter physics. It underlies the fundamental concept of polaron quasiparticle [1] and manifests in a variety of intriguing quantum many-body phenomena, including Anderson orthogonality catastrophe [2], the Fermi edge singularity in the x-ray absorption of metals [3, 4], and Nagaoka ferromagnetism [5]. In the past two decades, there is a resurgence of interests on this traditional Fermi polaron problem, due to the rapid advances in ultra-cold atomic physics [6–8]. By tuning the interatomic interactions of a highly spin-population imbalanced two-component Fermi gas [9, 10], spectral properties of Fermi polarons in two and three dimensions can now be routinely measured using radio-frequency spectroscopy [11–13], Ramsey interferometry [14], Rabi cycle [15, 16], and Raman spectroscopy [17], with unprecedented accuracy. At low momentum, the observed spectral features such as the excited repulsive polaron branch and molecule-hole continuum have been well explained by variational Chevy ansatz [18–21], diagrammatic theories [22–26], functional renormalization group [27, 28], Monte Carlo simulations [29–31] and exactly solvable models in the heavy polaron limit [32–34].

In this Letter, by exactly calculating the spectral function based on the integrable one-dimensional (1D) Hubbard model [35–37], we show that additional distinct characteristics of Fermi polarons, such as anomalous Fermi singularities (see the features I and III in Fig. 1) in coexistence with polaron quasiparticles (see the features II and IV), could arise in 1D lattices at large impurity momentum. These new features are entirely not anticipated. The 1D Fermi polaron is often considered to be trivial, since Anderson orthogonality catastrophe survives for a mobile impurity in one-dimension and therefore Fermi edge singularities are expected to appear in the impurity

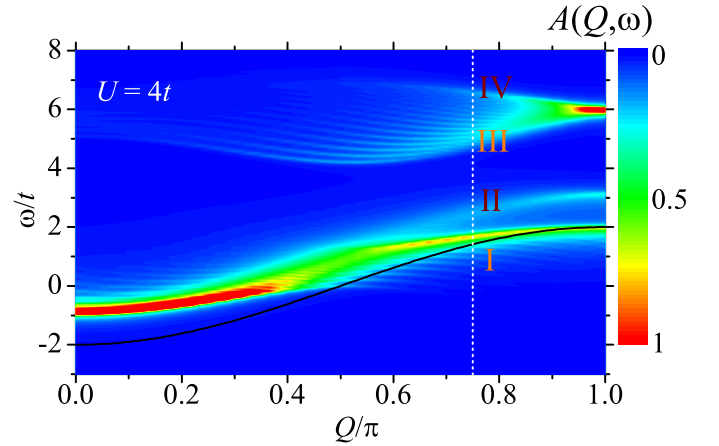


FIG. 1. The contour plot of the impurity spectral function $A(Q, \omega)$, in units of the inverse hopping strength t^{-1} . The black line shows the bare impurity dispersion relation $\varepsilon_Q = -2t \cos Q$. Along the cut at the momentum $Q = 0.75\pi$, as indicated by the vertical dotted line, we may identify four spectral features I, II, III and IV, to be discussed in detail in Fig. 3. Here, we consider a quarter filling $\nu = (N+1)/L = 0.5$ with $L = 80$ and take an on-site repulsion $U = 4t$.

spectral function. This idea was partly examined in Ref. [38] by calculating the ground-state form factor of the exactly solvable continuous Gaudin-Yang model [39].

Here, we generalize the pioneering work [38] to the 1D Hubbard model and calculate the form factors of all the excited many-body states, including the spin-flip state and η -pairing state [40] that are not covered by regular Bethe wavefunctions [36, 41]. This enables us to exactly determine the impurity spectral function at finite on-site repulsions $U \neq \infty$ for the first time. At low momentum, we observe the conventional Fermi edge singularities, as already clarified by the calculation of the ground-state

form factor [38]. With increasing momentum these Fermi singularities gradually turn into two-sided singularities and eventually become anomalous with low-energy oriented power-law tails, upon reaching the boundary of Brillouin zone. Most interestingly, polaron quasiparticles contributed by a collection of excited many-body states start to appear, when the filling factor of the Fermi bath is about quarter.

In addition to providing benchmark results for approximate theories on Fermi polarons, our exact predictions of new distinct polaron spectral features could be directly examined in the future cold-atom experiments. Our technique of determining the form factor is useful to study exact dynamics of impurity in a lattice Fermi bath such as quantum flutter [42–46] in lattices. It may also be generalized to the case of several impurities, so the effective bath-induced interactions between polaron quasiparticles and Fermi singularities might be elucidated in the impurity spectral function. In this case, we may also anticipate to see the emergence of the spin degree of freedom and the demonstration of the peculiar spin-charge separation in the spectrum [36, 37, 47].

Regular Bethe wavefunctions. We start by considering the well-known Bethe ansatz solution $|\Psi_{N+1,Q}\{k_j, \Lambda\}\rangle$ of the 1D Hubbard model with N spin-up fermions and one spin-down fermion (i.e., the impurity) on a lattice with an even number of sites $L \geq N$ [35, 36]:

$$\sin k_j - \Lambda = u \cot \left(\frac{k_j L}{2} \right), \quad (1)$$

where $u = U/(4t)$ is the dimensionless interaction parameter, $Q = \sum_{j=1}^{N+1} k_j \pmod{2\pi}$ is the total momentum, and each real quasi-momentum k_j can be uniquely characterized by an integer $s_j \in [-L/2 + 1, L/2]$ in the region $(s_j - 1)2\pi/L \leq k_j < s_j 2\pi/L$ [48, 49]. In the case of a single impurity, the quasi-momentum Λ related to the impurity position is always real. In contrast, a complex-valued pair of the quasi-momenta (k_1 and $k_2 = k_1^*$, for clarity) may arise even for repulsive interaction $u > 0$, due to the existence of two-body bound states [36]. Thus, we classify the whole regular Bethe wavefunctions with finite quasi-momenta into two types [36]: the real- k solutions and the $k - \Lambda$ solutions (with a complex-valued pair of quasi-momenta k_1 and k_2).

For the given set of integers $\{s_j\}$, Eq. (1) can be easily solved for each momentum k_j , with an adjustable Λ to reproduce the given total momentum Q [49]. At a repulsive on-site interaction $u > 0$, the ground state has $s_j = -(N+1)/2 + j$ for an odd N (see Fig. (3a)), which might be visualized as a pseudo Fermi sea. The set of $\{s_j\}$ for an arbitrary excited many-body state can then be uniquely specified by listing pseudo particle-hole pairs relative to the fully occupied pseudo Fermi sea. Typically, the energy $E_{N+1}(\{k_j\}, \Lambda) = -2t \sum_{j=1}^{N+1} \cos k_j$ will increase with creating more particle-hole pairs.

Once we solve the quasi-momenta $\{k_j\}$ and Λ , it is straightforward to write the regular Bethe wavefunction (with a normalization factor C_Ψ) into a determinant,

$$|\Psi_{N+1,Q}\{k_j, \Lambda\}\rangle = C_\Psi \sqrt{\frac{1}{N!L}} e^{iQx_\downarrow} \det_{1 \leq j, m \leq N} [\phi_j(y_m)], \quad (2)$$

where x_\downarrow is the position of the impurity and $y_m = x_m - x_\downarrow$ is the coordinate of the m -th spin-up fermion relative to the impurity, and $\phi_j(y) \equiv \chi_j(y) - \chi_{N+1}(y)$ with the wavefunction $\chi_j(y) = [\Lambda - \sin(k_j) + iu]e^{ik_j y}/(u\sqrt{L})$. This elegant determinant form of the Bethe wavefunction was first suggested by Edwards [50] and later was used to address the Fermi edge singularity [38] and quantum flutter [42] in the Gaudin-Yang model. Here, we adopt a single-particle wavefunction $\chi_j(y)$ that is more suitable to handle the $k - \Lambda$ solutions with a pair of complex-valued quasi-momenta [51].

Form factor. We are interested in the form factor or the overlap $F_{N+1}(\{k_j\}, \Lambda)$ of the Bethe wavefunction with the product state of the impurity plane-wave (with momentum Q) and a non-interacting Fermi sea, which also takes the form of a Slater determinant in the first quantization, i.e., $\psi_{Q\downarrow}^\dagger |\text{FS}_N\rangle = e^{iQx_\downarrow} \det_{1 \leq j, m \leq N} [e^{iq_j y_m}/\sqrt{L}]/\sqrt{N!L}$, where $q_j = [-(N+1)/2 + j]2\pi/L$. This overlap of two Slater determinants can be readily obtained, following a well-known identity in quantum chemistry [52],

$$F_{N+1}(\{k_j\}, \Lambda) = C_\Psi \begin{vmatrix} B_{11} & \cdots & B_{1N} & B_{1,N+1} \\ \vdots & \vdots & \vdots & \vdots \\ B_{N1} & \cdots & B_{NN} & B_{N,N+1} \\ 1 & \cdots & 1 & 1 \end{vmatrix}, \quad (3)$$

where the matrix element $B_{jl} \equiv [e^{-iq_j} + e^{ik_l}]/[L(\sin q_j - \sin k_l)]$. Using the same identity, we find the normalization factor, $C_\Psi = [s_{k\Lambda} u_1 u_2 \cdots u_{N+1} (u_1^{-1} + u_2^{-1} + \cdots + u_{N+1}^{-1})]^{-1/2}$, where $u_j \equiv 1 + (\sin k_j - \Lambda)^2/u^2 + 2 \cos k_j/(Lu)$ and a minus sign $s_{k\Lambda} = -1$ arises for the $k - \Lambda$ solutions. By introducing the residue $Z_{N+1}(\{k_j\}, \Lambda) \equiv |F_{N+1}(\{k_j\}, \Lambda)|^2$, we obtain the spectral function,

$$A(Q, \omega) = -\frac{\text{Im}}{\pi} \sum_{\{k_j\}, \Lambda} \frac{Z_{N+1}(\{k_j\}, \Lambda)}{\omega - E_{N+1}(\{k_j\}, \Lambda) + E_{\text{FS},N} + i\delta}, \quad (4)$$

where $E_{\text{FS},N}$ is the energy of the non-interacting Fermi sea $|\text{FS}_N\rangle$ and $\delta \equiv 4t/L$ is a broadening factor used to smooth the discrete energy levels at finite L .

Irregular states. The sum in the above spectral function should be over all the many-body wavefunctions, including some irregular states that are not covered by the regular Bethe wavefunctions [36, 41]. Fortunately, these irregular states can be directly constructed by acting a spin-flip operator $\zeta^\dagger \equiv \sum_k \psi_{k\downarrow}^\dagger \psi_{k\uparrow}$ and an η -pairing operator $\eta^\dagger \equiv \sum_k \psi_{k\downarrow}^\dagger \psi_{\pi-k\uparrow}^\dagger$ on some non-interacting

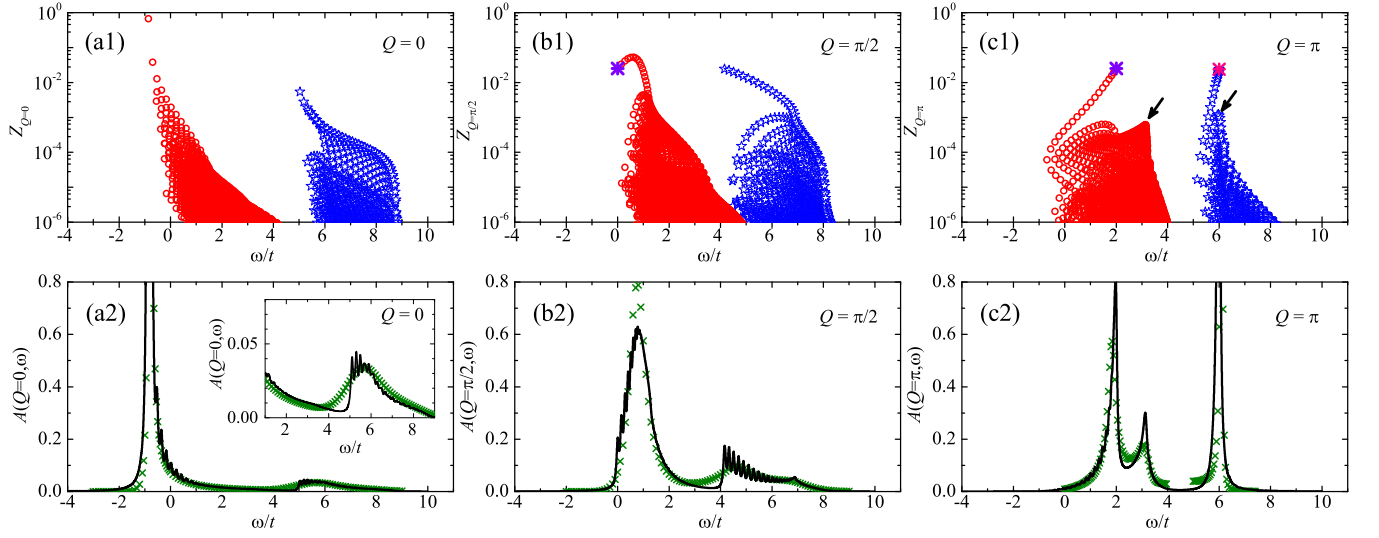


FIG. 2. Residues (a1, b1 and c1) and the impurity spectral functions (a2, b2 and c2, in units of t^{-1}) as a function of the energy $E_{N+1} - E_{FS,N}$ or ω , at different momentum as indicated. In the upper panel, the residues of the real- k solutions and the $k - \Lambda$ solutions are shown by red circles and blue stars, respectively. The eight-spoked asterisks show the residues of the spin-flip state and of the η -pairing state. In the lower panel, the green crosses show the spectral functions predicted by the variational Chevy ansatz with two-particle-hole excitations [26] (see Appendix A for more details). The inset in (a2) highlights the high-energy Fermi singularity.

states [36, 41]. By inspection, we may explicitly determine the relevant spin-flip state and η -pairing state, $\Psi_\zeta = C_\zeta \zeta^\dagger \psi_{Q\uparrow}^\dagger |\text{FS}_N\rangle$ and $\Psi_\eta = C_\eta \eta^\dagger \psi_{\pi-Q\uparrow}^\dagger |\text{FS}_N\rangle$, with energy $E_\zeta - E_{FS,N} = -2t \cos Q$ and $E_\eta - E_{FS,N} = -2t \cos Q + U$ and with form factor $F_\zeta = C_\zeta = 1/\sqrt{N+1}$ and $F_\eta = C_\eta = 1/\sqrt{L-N+1}$, respectively. From the wavefunctions, it is easy to see that the spin-flip state or η -pairing state exists only when the momentum Q is out of the Fermi sea (i.e., $Q \notin \{q_j\}$) or the momentum $\pi - Q$ is in the Fermi sea ($\pi - Q \in \{q_j\}$). It is worth noting that when the irregular states exist, we can use the sum rule $\varrho_s = F_\zeta^2 + F_\eta^2 + \sum_{\{k_j\}, \Lambda} Z_{N+1}(\{k_j\}, \Lambda) = 1$ to examine the completeness of the many-body wavefunctions included in the numerical calculations [42].

Spectral function. We calculate the impurity spectral function for various lattice sizes, filling factors and on-site interactions. We keep up to three pseudo particle-hole pairs and sum over about half a million excited states (i.e., for the typical case of $L = 80$, $\nu = (N+1)/L = 0.5$ and $U = 4t$ unless stated otherwise) with $\varrho_s > 99.8\%$, so the omitted states have negligible effect on the convergence of our numerics.

In Fig. 2, we report the residues of all the many-body states (upper panel) and the related spectral function (lower panel) at different total momentum [53]. For residues, the real- k states and the $k - \Lambda$ solutions form two clusters, roughly separated in energy by the on-site repulsion $U = 4t$. Interestingly, the distributions of the residues in each cluster are qualitatively similar. At zero momentum $Q = 0$, the ground-state residue is dominant [38], followed by a series of states with rapidly decreasing

residues, thus leading to a sharp Fermi edge singularity at the threshold $\omega_0 \simeq -t$. In the $k - \Lambda$ cluster, there is a similar lowest-energy pair state but with a residue $Z \sim 0.01$, giving rise to a much weaker high-energy Fermi singularity at another threshold $\omega_1 \sim 5t$, as highlighted in the inset of Fig. 2(a2). These observations provide a direct confirmation of the existence of Fermi edge singularities in the spectral function of 1D Fermi polarons, as suggested in Ref. [38].

As the total momentum Q becomes larger than the Fermi wavevector $k_F = N\pi/L$, the residue distributions in the two clusters significantly change. In particular, the lowest-energy state in each cluster may no longer have the largest residue. Instead, a branch of states, involving also the irregular spin-flip state and η -pairing state, starts to contribute most significantly, as we shall analyze in detail. At $Q = \pi/2$ as illustrated in Figs. 2(b1) and 2(b2), this creates a two-sided Fermi singularity in each cluster. As the momentum Q increases further, the shape of the two-sided Ferm singularity changes. Upon reaching the boundary of the Brillouin zone at $Q = \pi$, we find that either the spin-flip state at $\omega = -2t \cos Q = 2t$ or the η -pairing state at $\omega = 2t + U$ becomes the state of the largest residue (see, i.e., the eight-spoked asterisks in Fig. 2(c1)). As a consequence, the high-energy side of the two-sided singularity disappears, leaving an anomalous Fermi singularity with a power-law tail extending to the low-frequency.

Remarkably, at $Q = \pi$ we observe an additional peak at $\omega \sim 3t$, just above the lower anomalous Fermi singularity at $\omega = 2t$, as shown in Fig. 2(c2). From the residue

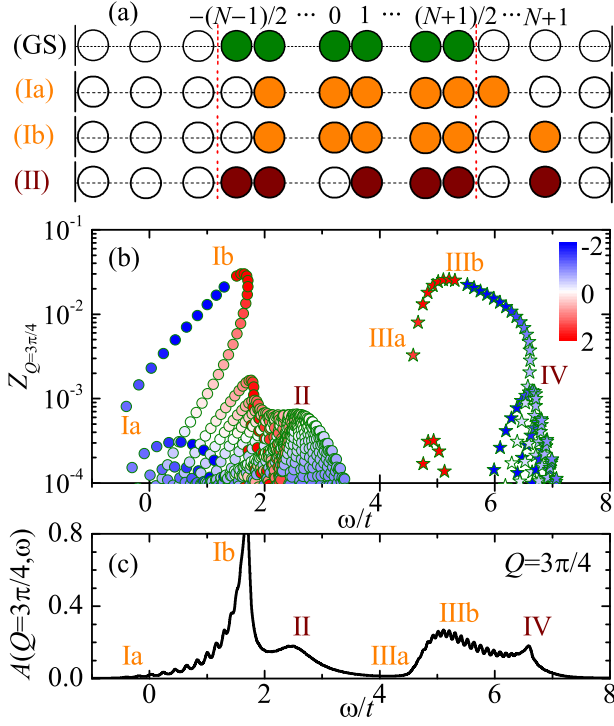


FIG. 3. Residues (b) and the impurity spectral function (c, in units of t^{-1}) at the momentum $Q = 3\pi/4$. The color in the symbols for residues shows the value of the quasi-momentum Λ , as indicated by the color-map. The four types of excitations have been denoted by the Roman numerals I, II, III and IV. The types Ia, Ib and II are explained diagrammatically in (a), with an illustration of the ground state (GS) distribution.

distributions, it is clear that this peak comes from a bundle of many-body states with a similar residue $Z \sim 10^{-3}$, as indicated by the left arrow in Fig. 2(c1). Although the residue is small, the number of the many-body states is sufficiently large to make the peak visible. This collective nature clearly suggests that the peak is a polaron quasiparticle, rather than a Fermi singularity. In the $k - \Lambda$ cluster, we also find a similar bundle of many-body states at $\omega = 6t$ with $Z \sim 10^{-3}$ (see the arrow on the right). However, their contributions seem to be covered up by the anomalous Fermi singularity exactly located at the same energy.

Nature of singularities and polarons. The observation of the anomalous Fermi singularities at large Q , coexisting with the polaron peaks, is the key result of our Letter. The evolution of these intriguing features with increasing momentum is displayed in the two-dimensional contour plot Fig. 1. To better understand how these features arise, we make a cut in the contour plot at $Q = 3\pi/4$ and present the corresponding residues and spectral function in Fig. 3. For the residues shown by symbols in Fig. 3(b), we assign different colors to indicate the value of the quasi-momentum Λ .

We find that the two branches of states that lead

to the anomalous Fermi singularity (I) and the two-sided singularity (III) are well-characterized by the one pseudo particle-hole excitations (i.e., holon-antiholon pair [36, 47]). For example, focusing on the singularity I, the two states labelled by Ia and Ib in Fig. 3(b) are obtained by removing the leftmost hole state with $s_j = -(N-1)/2$ in the pseudo Fermi sea (GS) and then by occupying the particle state $s_j = (N+1)/2 + 1$ and $s_j = N+1$, respectively, as shown in Fig. 3(a). These branches of states are asymmetrically distributed in $\{s_j\}$ compared with the pseudo Fermi sea, and hence have a significant overlap with the product state $\psi_{Q\downarrow}^\dagger |\text{FS}_N\rangle$ that is asymmetric itself. We find that such an asymmetry in the distribution $\{s_j\}$ is indirectly evidenced by a large value of the quasi-momentum $|\Lambda|$.

In contrast, the polaron peak II is contributed by the many-body states with nearly zero quasi-momentum $|\Lambda| \sim 0$ (as indicated by the white color of the symbols), which suggests a symmetric distribution in $\{s_j\}$. As illustrated at the bottom of Fig. 3(a), these many-body states are constructed by relocating the hole states with $s_j \sim 0$ to the particle states with $s_j \sim N+1$, reminiscent of the bottom-of-band excitations observed in heavy Fermi polarons (see, i.e., Fig. 6(b) in Ref. [7]). Their residues are small but the number of such many-body states is large, due to many different ways of relocation. We note that, the many-body states forming the polaron II can hardly be understood as the spinon excitations, which correspond to the change of a quantum number J that characterizes the quasi-momentum Λ . However, for multiple impurities, where a spinon Fermi sea forms, the spinon excitations would show up in the spectral function near $Q = 0$ (or $Q = \pi$) in the lower (or upper) Hubbard band [47], signaling spin-charge separation.

To further elucidate the existence of singularities and polarons, we perform a finite-size-scaling analysis of the maximum values A_{\max} for the three peaks in Fig. 2(c2). By calculating A_{\max} at different length ($L = 20, 40, 60$ and 80) with a broadening factor $\delta = 4t/L$, we anticipate a constant A_{\max} for polarons or a divergent A_{\max} in the form of $\delta^{-\alpha}$ ($0 < \alpha < 1$) for singularities as $\delta \rightarrow 0$. We find $\alpha = 0.50$ and $\alpha = 0.89$ for the first and third peaks, indicating their nature as Fermi singularities. Instead, we obtain a much smaller exponent $\alpha = 0.31$ for the second peak at $\omega \sim 3t$, which is more consistent with the interpretation of a polaron quasiparticle. More details are given in Appendix B.

We finally note that, the co-existence of singularities and polarons at $Q \sim \pi$ take place only near the quarter filling factor $\nu = 1/2$. This might be related to the backward scattering between the two Fermi points, which becomes favourable when the transferred momentum $2k_F \sim \pi \sim Q$. In the dilute limit (see Fig. 4(a) for $\nu = 0.2$), the separated clustering of the many-body states for the polaron quasiparticle, as indicated by II in Fig. 3(b), does not occur. Near the half filling (Fig.

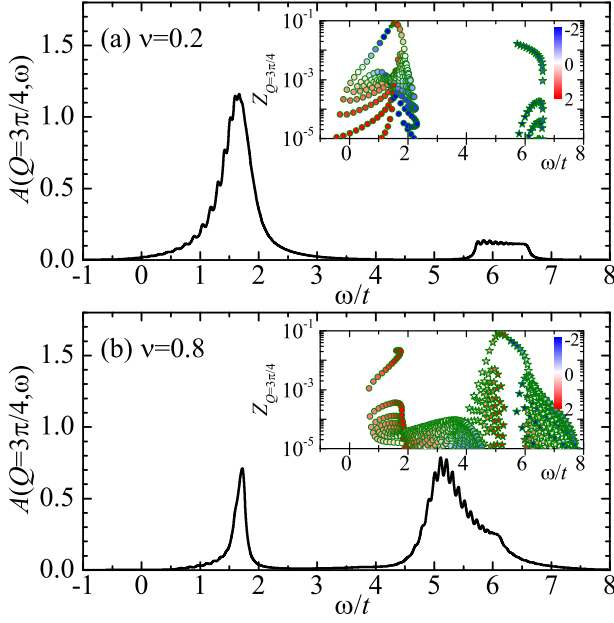


FIG. 4. Impurity spectral functions, in units of t^{-1} , at two filling factors $\nu = 0.2$ (a) and $\nu = 0.8$ (b) and at the momentum $Q = 3\pi/4$. The insets show the distribution of the residues, with increasing energy.

4(b)), the clustering does happen. However, the residues of the many-body states are too small to form a visible polaron peak.

Conclusions. In summary, we have calculated the exact spectral function of one-dimensional Fermi polarons in lattices, by using the celebrated Bethe wavefunctions [36]. We have found the coexistence of anomalous Fermi singularity and polaron quasiparticles at large momentum near the quarter filling. This interesting feature could be experimentally observed with ultracold atoms using Ramsey interferometry [45], in which the impurity can be first accelerated to acquire momentum Q [54] and the consequently measured Ramsey overlap function $S(t)$ gives rise to the spectral function $A(Q, \omega)$ after a Fourier transformation [7, 32]. Further extension of our work with multiple impurities would be useful to explore polaron-polaron interactions and the emergence of spin-charge separation in one dimension [37, 47].

Acknowledgments. This research was supported by the Australian Research Council's (ARC) Discovery Program, Grants Nos. DP240101590 (H.H.), FT230100229 (J.W.), and DP240100248 (X.-J.L.).

Appendix A: Spectral function from Chevy ansatz approach

In previous works, the polaron spectral function has been calculated by using various approximate approaches, including variational Chevy ansatz and many-

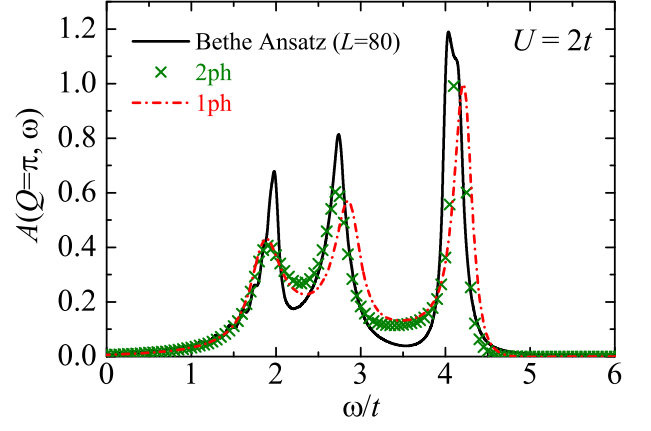


FIG. 5. Impurity spectral function $A(Q = \pi, \omega)$ predicted by using variational Chevy ansatz, with one-particle-hole excitations (red dot-dashed line) and with two-particle-hole excitations (green crosses) [26] in the thermodynamic limit, with a broadening factor δ extrapolated to zero. Here, we take the on-site repulsion $U = 2t$. For the Bethe ansatz calculation, the number of spin-up atoms is $N = 39$ and the number of sites is $L = 80$.

body diagrammatic theory [26]. In the lower panel of Fig. 2, we have compared the exact predictions from Bethe ansatz (solid lines) with the results from variational Chevy ansatz with the inclusion of two-particle-hole excitations (green crosses). In Fig. 5, we present an additional comparison at the on-site repulsion $U = 2t$, including the variational results with both one-particle-hole excitations (see the red dot-dashed line) and two-particle-hole excitations.

Using the exact Bethe ansatz results as a benchmark, we find that the inclusion of two-particle-hole excitations quantitatively improves the predictive power of the variational Chevy ansatz. In particular, the polaron peak in the middle seems to be well-reproduced by the Chevy ansatz approach with two-particle-hole excitations.

Appendix B: Finite-size-scaling analysis

In the main text, we have stated that the maximum value A_{\max} of a Fermi singularity scales as, $A_{\max} \propto \delta^{-\alpha}$, where $\delta = 4t/L$ is the broadening factor and the exponent α satisfies $0 < \alpha < 1$. For the polaron peak, we instead anticipate a constant A_{\max} , independent of the number of sites L (i.e., $\alpha \sim 0$).

To check this scaling law, in Fig. 6(a) we plot $\ln A_{\max}$ as a function of $\ln \delta$ for the Fermi-edge singularity at $Q = 0$ and at $U = 4t$ and half filling $\nu = 0.5$. In this case, the exponent α is analytically given by [38],

$$\alpha = 1 - 2 \left(\frac{\delta'_F}{\pi} \right)^2, \quad (\text{B1})$$

where the phase shift δ'_F is related to the on-site repulsion

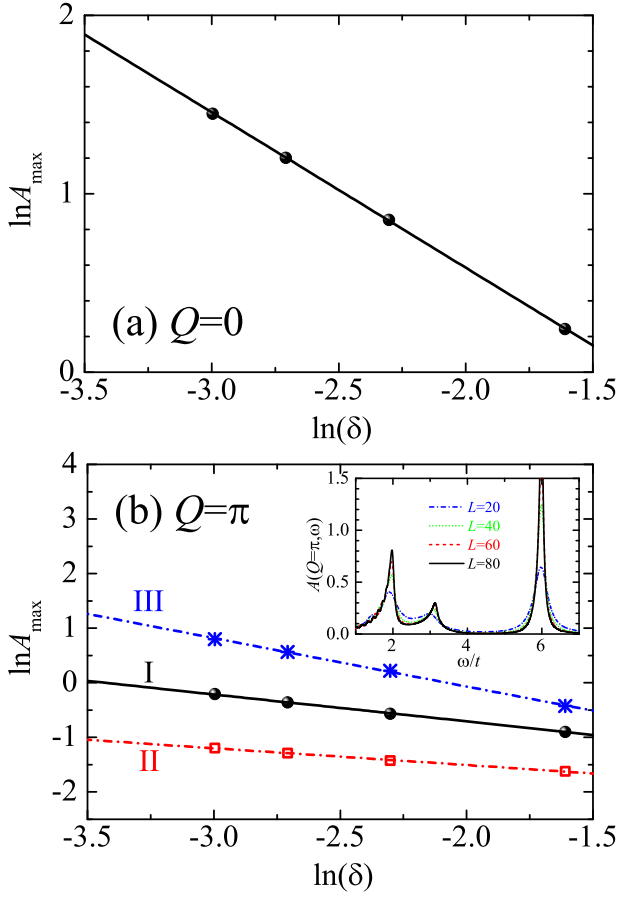


FIG. 6. $\ln A_{\max}$ as a function of $\ln \delta$, for the $Q = 0$ singularity (a) and for the singularities (I and III) and the polaron peak (II) at $Q = \pi$ (b). The lines are the linear fits, $\ln A_{\max} = -\alpha \ln \delta + \text{const}$, to the data points. The inset in (b) reports the spectral function at different number of sites L . Here, we consider a quarter filling $\nu = (N + 1)/L = 0.5$ and an on-site repulsion $U = 4t$.

by, $\delta'_F = -\arctan(\pi U n_F/2)$, where $n_F = 1/(2\pi t \sin k_F)$ is the density of state at the Fermi point and $k_F = \nu\pi$ is the Fermi wavevector. By substituting $U = 4t$ into the expressions, we find that the phase shift $\delta'_F = -\pi/4$ and hence the exponent $\alpha = 7/8 = 0.875$. Numerically, by linearly fitting the data in Fig. 6(a), we obtain from the slope $\alpha_{\text{fit}} = 0.871$, which is very close to the expected value of $\alpha = 0.875$.

The linear fits for the anomalous Fermi singularities (I and III) and the polaron peak (II) at $Q = \pi$ are reported in Fig. 6(b). The exponent for the polaron peak (II), $\alpha_{\text{II}} = 0.31$, is small but nonzero. This is probably due to the fact that the polaron peak (II) is not completely separated from the Fermi singularity (I) due to a finite broadening factor δ . The finite overlap then may bring a weak L -dependence to the polaron peak value A_{\max} .

To reduce the overlap, we take a smaller broadening factor $\delta = t/L$ with $L = 60, 80$ and 100 for the collective peak (II), as shown in Fig. 7. The numerical fit of the

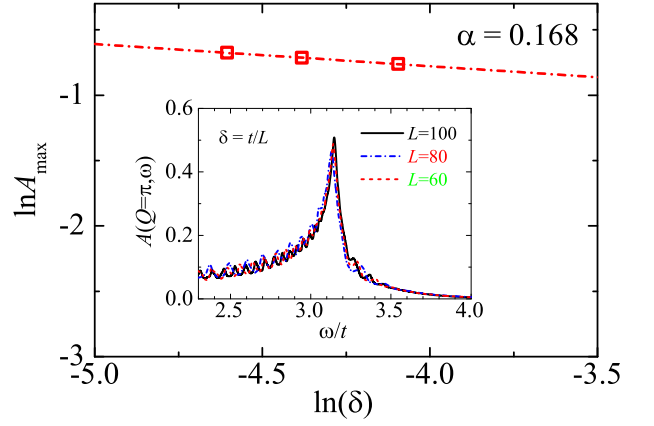


FIG. 7. $\ln A_{\max}$ as a function of $\ln \delta$, for the the polaron peak (II) at $Q = \pi$, where we take a smaller broadening factor $\delta = t/L$. The linear fit (i.e., $\ln A_{\max} = -\alpha \ln \delta + \text{const}$), as given by the red dot-dashed line, leads to an exponent $\alpha_{\text{II}} \simeq 0.17$. The inset reports the spectral function at different number of sites L for the polaron peak (II). The other parameters are the same as in Fig. 6.

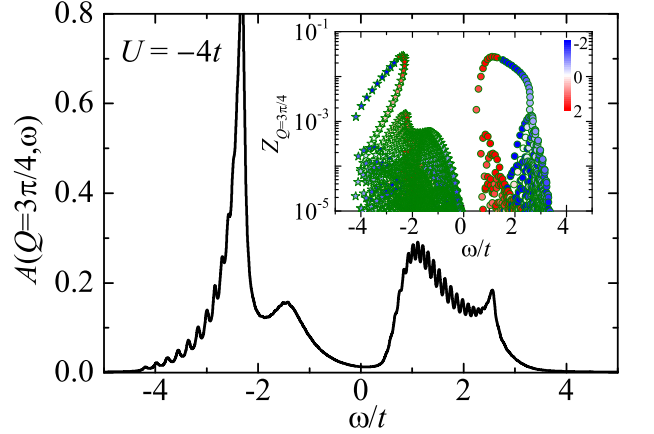


FIG. 8. Impurity spectral function $A(Q = 3\pi/4, \omega)$ at an attractive on-site interaction $U = -4t$. As in Fig. 3(c), we consider a quarter filling $\nu = (N + 1)/L = 0.5$ with $L = 80$.

data $\ln A_{\max}$ leads to an exponent $\alpha_{\text{II}} = 0.17$. As anticipated, this exponent is indeed smaller than the value of 0.31 , obtain with $\delta = 4t/L$. It is reasonable to believe that, by taking the limit $\delta \rightarrow 0$ with more numerical efforts, we might eventually confirm $\alpha_{\text{II}} = 0$ for the polaron peak (II).

Appendix C: Attractive on-site interaction

Here, we also examine the case of an attractive on-site interaction. In Fig. 8, we show the impurity spectral function $A(Q = 3\pi/4, \omega)$ at $U = -4t$, keeping other parameters the same as in Fig. 3(c). Interestingly, we find the qualitative same spectral function as in the case of on-

site repulsion $U = 4t$, in spite of a constant energy shift around $4t$. Therefore, the coexistence of the anomalous Fermi singularities and polaron quasiparticles seems to be a robust and universal feature of Fermi polaron in 1D lattices, regardless of the sign of on-site interactions.

This similarity can be easily understood by performing a particle-hole transformation for the Fermi bath (i.e., spin-up fermions), $\psi_{i\downarrow}^\dagger \rightarrow (-1)^i \psi_{i\downarrow}$, under which the single-particle kinetic Hamiltonian is invariant and up to a constant energy shift the interaction Hamiltonian acquires a minus sign, i.e., $U \rightarrow -U$. The filling factor of the Fermi bath changes as, $\nu \rightarrow 1 - \nu$. Therefore, the polaron problem at the repulsion ($+U$) at the filling factor ν is identical to the case of an attractive interaction ($-U$) at the filling factor $1 - \nu$, if we neglect the unimportant energy shift.

-
- [1] A. S. Alexandrov and J. T. Devreese, *Advances in Polaron Physics* (Springer, New York, 2010), Vol. 159.
 - [2] P. W. Anderson, Infrared Catastrophe in Fermi Gases with Local Scattering Potentials, *Phys. Rev. Lett.* **18**, 1049 (1967).
 - [3] G. D. Mahan, Excitons in Metals: Infinite Hole Mass, *Phys. Rev.* **163**, 612 (1967).
 - [4] P. Nozières and C. T. De Dominicis, Singularities in the X-Ray Absorption and Emission of Metals. III. One-Body Theory Exact Solution, *Phys. Rev.* **178**, 1097 (1969).
 - [5] Y. Nagaoka, Ferromagnetism in a Narrow, Almost Half-Filled s Band, *Phys. Rev.* **147**, 392 (1966).
 - [6] P. Massignan, M. Zaccanti, and G. M. Bruun, Polarons, dressed molecules and itinerant ferromagnetism in ultracold Fermi gases, *Rep. Prog. Phys.* **77**, 034401 (2014).
 - [7] R. Schmidt, M. Knap, D. A. Ivanov, J.-S. You, M. Cetina, and E. Demler, Universal many-body response of heavy impurities coupled to a Fermi sea: a review of recent progress, *Rep. Prog. Phys.* **81**, 024401 (2018).
 - [8] J. Wang, Functional determinant approach investigations of heavy impurity physics, *AAPPS Bull.* **33**, 20 (2023).
 - [9] I. Bloch, J. Dalibard, and W. Zwerger, Many-body physics with ultracold gases, *Rev. Mod. Phys.* **80**, 885 (2008).
 - [10] C. Chin, R. Grimm, P. Julienne, and E. Tiesinga, Feshbach resonances in ultracold gases, *Rev. Mod. Phys.* **82**, 1225 (2010).
 - [11] A. Schirotzek, C.-H. Wu, A. Sommer, and M.W. Zwierlein, Observation of Fermi Polarons in a Tunable Fermi Liquid of Ultracold Atoms, *Phys. Rev. Lett.* **102**, 230402 (2009).
 - [12] Y. Zhang, W. Ong, I. Arakelyan, and J. E. Thomas, Polaron-to-Polaron Transitions in the Radio-Frequency Spectrum of a Quasi-Two-Dimensional Fermi Gas, *Phys. Rev. Lett.* **108**, 235302 (2012).
 - [13] Z. Yan, P. B. Patel, B. Mukherjee, R. J. Fletcher, J. Struck, and M.W. Zwierlein, Boiling a Unitary Fermi Liquid, *Phys. Rev. Lett.* **122**, 093401 (2019).
 - [14] M. Cetina, M. Jag, R. S. Lous, I. Fritsche, J. T. M. Walraven, R. Grimm, J. Levinsen, M. M. Parish, R. Schmidt, M. Knap, and E. Demler, Ultrafast many-body interferometry of impurities coupled to a Fermi sea, *Science* **354**, 96 (2016).
 - [15] F. Scazza, G. Valtolina, P. Massignan, A. Recati, A. Amico, A. Burchianti, C. Fort, M. Inguscio, M. Zaccanti, and G. Roati, Repulsive Fermi Polarons in a Resonant Mixture of Ultracold ^6Li Atoms, *Phys. Rev. Lett.* **118**, 083602 (2017).
 - [16] F. J. Vivanco, A. Schuckert, S. Huang, G. L. Schumacher, G. G. T. Assumpção, Y. Ji, J. Chen, M. Knap, and Nir Navon, The strongly driven Fermi polaron, arXiv:2308.05746.
 - [17] G. Ness, C. Shkedrov, Y. Florshaim, O. K. Diessel, J. von Milczewski, R. Schmidt, and Y. Sagi, Observation of a Smooth Polaron-Molecule Transition in a Degenerate Fermi Gas, *Phys. Rev. X* **10**, 041019 (2020).
 - [18] F. Chevy, Universal phase diagram of a strongly interacting Fermi gas with unbalanced spin populations, *Phys. Rev. A* **74**, 063628 (2006).
 - [19] R. Combescot and S. Giraud, Normal State of Highly Polarized Fermi Gases: Full Many-Body Treatment, *Phys. Rev. Lett.* **101**, 050404 (2008).
 - [20] M. M. Parish and J. Levinsen, Highly polarized Fermi gases in two dimensions, *Phys. Rev. A* **87**, 033616 (2013).
 - [21] W. E. Liu, J. Levinsen, and M. M. Parish, Variational Approach for Impurity Dynamics at Finite Temperature, *Phys. Rev. Lett.* **122**, 205301 (2019).
 - [22] R. Combescot, A. Recati, C. Lobo, and F. Chevy, Normal State of Highly Polarized Fermi Gases: Simple Many-Body Approaches, *Phys. Rev. Lett.* **98**, 180402 (2007).
 - [23] H. Hu, B. C. Mulkerin, J. Wang, and X.-J. Liu, Attractive Fermi polarons at nonzero temperatures with a finite impurity concentration, *Phys. Rev. A* **98**, 013626 (2018).
 - [24] H. Tajima and S. Uchino, Thermal crossover, transition, and coexistence in Fermi polaronic spectroscopies, *Phys. Rev. A* **99**, 063606 (2019).
 - [25] H. Hu and X.-J. Liu, Fermi polarons at finite temperature: Spectral function and rf spectroscopy, *Phys. Rev. A* **105**, 043303 (2022).
 - [26] H. Hu, J. Wang, and X.-J. Liu, Theory of the spectral function of Fermi polarons at finite temperature, *Phys. Rev. Lett.* **133**, 083403 (2024).
 - [27] R. Schmidt and T. Enss, Excitation spectra and rf response near the polaron-to-molecule transition from the functional renormalization group, *Phys. Rev. A* **83**, 063620 (2011).
 - [28] J. von Milczewski and R. Schmidt, Momentum-dependent quasiparticle properties of the Fermi polaron from the functional renormalization group, *Phys. Rev. A* **110**, 033309 (2024).
 - [29] N. Prokof'ev and B. Svistunov, Fermi-polaron problem: Diagrammatic Monte Carlo method for divergent sign-alternating series, *Phys. Rev. B* **77**, 020408(R) (2008).
 - [30] O. Goulko, A. S. Mishchenko, N. Prokof'ev, and B. Svistunov, Dark continuum in the spectral function of the resonant Fermi polaron, *Phys. Rev. A* **94**, 051605(R) (2016).
 - [31] S. Ramachandran, S. Jensen, Y. Alhassid, Precision Thermodynamics of the Fermi polaron at strong coupling, arXiv:2410.00886.
 - [32] M. Knap, A. Shashi, Y. Nishida, A. Imambekov, D. A. Abanin, and E. Demler, Time-Dependent Impurity in Ultracold Fermions: Orthogonality Catastrophe and Beyond, *Phys. Rev. X* **2**, 041020 (2012).

- [33] J. Wang, X.-J. Liu, and H. Hu, Exact Quasiparticle Properties of a Heavy Polaron in BCS Fermi Superfluids, *Phys. Rev. Lett.* **128**, 175301 (2022).
- [34] J. Wang, X.-J. Liu, and H. Hu, Heavy polarons in ultracold atomic Fermi superfluids at the BEC-BCS crossover: Formalism and applications, *Phys. Rev. A* **105**, 043320 (2022).
- [35] E. H. Lieb and F. Y. Wu, Absence of Mott Transition in an Exact Solution of the Short-Range, One-Band Model in One Dimension, *Phys. Rev. Lett.* **20**, 1445 (1968).
- [36] T. Deguchi, F. H. L. Essler, F. Göhmann, A. Klümper, V. E. Korepin and K. Kusakabe, Thermodynamics and excitations of the one-dimensional Hubbard model, *Phys. Rep.* **331**, 197 (2000).
- [37] F. H. L. Essler, H. Frahm, F. Göhmann, A. Klümper, and V. E. Korepin, *The One-Dimensional Hubbard Model* (Cambridge University Press, New York, 2005).
- [38] H. Castella and X. Zotos, Exact calculation of spectral properties of a particle interacting with a one-dimensional fermionic system, *Phys. Rev. B* **47**, 16186 (1993).
- [39] J. B. McGuire, Interacting fermions in one dimension. II. Attractive potential, *J. Math. Phys.* **7**, 123 (1966).
- [40] C. N. Yang, η pairing and off-diagonal long-range order in a Hubbard model, *Phys. Rev. Lett.* **63**, 2144 (1989).
- [41] F. H. L. Essler, V. E. Korepin, and K. Schoutens, New eigenstates of the 1-dimensional Hubbard model, *Nucl. Phys. B* **372**, 559 (1992).
- [42] C. J. M. Mathy, M. B. Zvonarev, and E. Demler, Quantum flutter of supersonic particles in one-dimensional quantum liquids, *Nat. Phys.* **8**, 881 (2012).
- [43] M. Knap, C. J. M. Mathy, M. Ganahl, M. B. Zvonarev, and E. Demler, Quantum Flutter: Signatures and Robustness, *Phys. Rev. Lett.* **112**, 015302 (2014).
- [44] O. Gamayun, O. Lychkovskiy, E. Burovski, M. Malcomson, V. V. Cheianov, and M. B. Zvonarev, Impact of the Injection Protocol on an Impurity's Stationary State, *Phys. Rev. Lett.* **120**, 220605 (2018).
- [45] P. E. Dolgirev, Y.-F. Qu, M. B. Zvonarev, T. Shi, and E. Demler, Emergence of a Sharp Quantum Collective Mode in a One-Dimensional Fermi Polaron, *Phys. Rev. X* **11**, 041015 (2021).
- [46] Z.-H. Zhang, Y. Jiang, H.-Q. Lin, and Xi-Wen Guan, Microscopic origin of the quantum supersonic phenomenon in one dimension, *Phys. Rev. A* **110**, 023329 (2024).
- [47] M. Kohno, Spectral Properties near the Mott Transition in the One-Dimensional Hubbard Model, *Phys. Rev. Lett.* **105**, 106402 (2010).
- [48] In the literature, the quasi-momentum k_j is specified by a half integer I_j for odd number of N [36, 37, 47]. Our integer quantum number s_j is related to I_j by $s_j = I_j + 1/2$.
- [49] X.-J. Liu and H. Hu, Exact calculation of spectral properties of a particle interacting with a one-dimensional Fermi gas in optical lattices, *AAPPS Bull.* **35**, 9 (2025).
- [50] D. M. Edwards, Magnetism in Single-Band Models: Exact One-Dimensional Wave Functions Generalised to Higher Dimensions, *Prog. Theor. Phys. Suppl.* **101**, 453 (1990).
- [51] O. Gamayun, A. G. Pronko, and M. B. Zvonarev, Impurity Green's function of a one-dimensional Fermi gas, *Nucl. Phys. B* **892**, 83 (2015).
- [52] F. Plasser, M. Ruckebauer, S. Mai, M. Oppel, P. Marquetand, and L. González, Efficient and Flexible Computation of Many-Electron Wave Function Overlaps, *J. Chem. Theory Comput.* **12**, 1207 (2016).
- [53] There are small fast oscillations in the spectral function, due to the discrete eigenstates at finite number of lattice sites L , which can not completely smoothed out by the finite broadening factor $\delta = 4t/L$. These fast oscillations are not important and should disappear for sufficiently large L .
- [54] F. Meinert, M. Knap, E. Kirilov, K. Jag-Lauber, M. B. Zvonarev, E. Demler, and H.-C. Nägerl, Bloch Oscillations in the Absence of a Lattice, *Science* **356**, 945 (2017).